Title

In vivo characterization of the human glioblastoma infiltrative edge with label-free intraoperative fluorescence lifetime imaging.

Journal

Biomedical Optics Express, 14(5)

ISSN

2156-7085

Authors

Alfonso-Garcia, Alba
Anbunesan, Silvia Noble
Bec, Julien
et al.

Publication Date

2023-05-01

DOI

10.1364/boe.481304

Peer reviewed

Research Article | Vol. 14, No. 5 / 1 May 2023 / Biomedical Optics Express 2196
Biomedical Optics EXPRESS

In vivo characterization of the human glioblastoma infiltrative edge with label-free intraoperative fluorescence lifetime imaging

ALBA ALFONSO-GARCIA,[1] SILVIA NOBLE ANBUNESAN,[1] JULIEN BEC,[1] HAN SUNG LEE,[2] LEE-WAY JIN,[2] ORIN BLOCH,[3] AND LAURA MARCU[1,3,*]

[1]Biomedical Engineering Department, University of California, Davis, One Shields Ave, Davis, CA 95616, USA
[2]Pathology and Laboratory Medicine Department, University of California, Davis, 4400 V St, Sacramento, CA 95817, USA
[3]Neurological Surgery Department, University of California, Davis, 4860 Y St, Sacramento, CA 95817, USA
*lmarcu@ucdavis.edu

Abstract: Challenges in identifying a glioblastoma's infiltrative edge during neurosurgical procedures result in rapid recurrence. A label-free fluorescence lifetime imaging (FLIm) device was used to evaluate glioblastoma's infiltrative edge *in vivo* in 15 patients (89 samples). FLIm data were analyzed according to tumor cell density, infiltrating tissue type (gray and white matter), and diagnosis history (new or recurrent). Infiltrations in white matter from new glioblastomas showed decreasing lifetimes and a spectral red shift with increasing tumor cell density. Areas of high versus low tumor cell density were separated through a linear discriminant analysis with a ROC-AUC=0.74. Current results support the feasibility of intraoperative FLIm for real-time *in vivo* brain measurements and encourage refinement to predict glioblastoma infiltrative edge, underscoring the ability of FLIm to optimize neurosurgical outcomes.

1. Introduction

Glioblastoma (GBM) is the most common type of malignant primary brain tumors (49%) and the most devastating with an average of 7% 5-year survival [1]. Maximal surgical tumor resection is the standard treatment for GBM patients. Typically, this results in a median patient survival rate of 12-14 months [2]. Such poor prognosis is attributed to the highly infiltrative nature of GBM. Accurate identification of tumor tissue around the surgical resection margins during the surgical procedure would lead to maximizing the extent of resection, minimally compromising eloquent areas, which is key to prolonging patient survival [2,3]. However, despite continuous efforts and innovative detection technologies to identify infiltration areas, surgeons still lack reliable means to properly assess resection margins [4]. The overarching goal of this study is to evaluate whether a label-free fluorescence lifetime imaging (FLIm) device can be used to identify areas of the infiltrative edge, defined as the areas of infiltration with various densities of tumor cells spreading into the viable brain parenchyma, within the surgical resection margins.

Histopathological evaluation remains the gold standard to determine the presence of tumor cells, with clear limiting factors. Such an approach is invasive due to tissue removal and time- consuming; thus, impractical when assessing the entire resection bed during surgery. Neuronavigational guidance based on pre-operative MRI is standard practice to localize the tumor mass, but standard MRI often underestimates the GBM infiltrating edge [5]. Fluorescence guided surgery (e.g., 5-ALA-induced fluorescence [6], near-infrared imaging [7]) provides *in situ* visual feedback of the tumor mass location. Current implementation of these methods, however, rely on fluorescence intensity measurements, which are qualitative, and have low sensitivity at the

#481304 https://doi.org/10.1364/BOE.481304
Journal © 2023 Received 17 Nov 2022; revised 24 Mar 2023; accepted 29 Mar 2023; published 24 Apr 2023

Biomedical Optics EXPRESS

infiltrating edge [8,9]. Other emerging technologies for assessing the extent of resection include intraoprative MRI [10], intraoperative ultrasound [11], and Raman spectroscopy [12]. Raman spectroscopy has a remarkable biochemical specificity that can resolve tissue type and areas with dense or invading cancer cells with high accuracy [13]. Additionally, integration through biopsy needles has demonstrated good performance in distinguishing areas of high tumor cellularity from normal brain [14,15] in preliminary *in vivo* studies. However, spontaneous Raman signals are weak and require longer integration times compared to fluorescence. With FLIm each point measurement is acquired in less than 1 μs, enabling free-hand scanning over large areas of tissue to minimize sampling error [16]. Moreover, unlike the Raman spectroscopy approaches currently available, FLIm does not require direct contact with tissue and can operate in the presence of any ambient light, allowing the surgeons to perform parallel imaging and resection work. On a different approach, stimulated Raman scattering was used to examine freshly excised brain tumor specimens in the operating room to recapitulate H&E stained tissue sections for histopathological evaluation (aka., stimulated Raman histology) to identify infiltration zones [17], and diagnose glioma types [18] with microscopic resolution.

FLIm has been integrated with the surgical workflow in the neurosurgical suite [19]] and has also demonstrated ability to discriminate between brain tissue types and lesions [19–23] based on tissue endogenous fluorescence, most notably from the emission of NAD(P)H and FAD, lipids, and porphyrins [24]. However, the FLIm signatures across the gradient of tumor cell densities in the infiltrative edge remain to be characterized. Implementing intraoperative FLIm through free-hand scanning of the surgical cavity enables rapid data acquisition from suspicious areas at the resection margins that can be ad hoc selected as the surgery progresses. Therefore, if FLIm can provide information on tumor cell density within the surgical resection margins, it could be an adjunct screening tool for neurosurgical procedures.

This study aimed 1) to characterize the FLIm signatures of GBM's infiltrative edge according to tumor cell density, tissue type the tumor infiltrates into (white matter versus gray matter), and diagnosis history (new versus recurrent GBM); and 2) to assess the potential of intraoperative FLIm to instantaneously detect areas of increased tumor density. The ability to identify areas with increased tumor cellularity around the resection margins in real-time could have a significant impact on GBM patients' surgical therapy and outcomes.

2. Materials and methods

2.1. Human patients

Fifteen patients diagnosed with glioblastoma (GBM), WHO grade IV, IDH wild-type were enrolled in this study. The study cohort consisted of 10 males and 5 females, with a median age of 58.1 (ranging between 43 -76). Twelve patients presented with newly diagnosed GBM, and three patients had recurrent GBM. Table 1 summarizes the patient demographic information and indicates the number of images/samples acquired/collected from each patient. A total of 89 tissue samples were further categorized as white matter or gray matter, according to their location. Informed consent was obtained from each patient before surgery. This study was approved by the University of California, Davis Institutional Review Board.

2.2. FLIm device

The FLIm instrument used in this study has been previously described [19,25]. A 355 nm pulsed laser (pulse duration <0.6 ns, pulse energy >2 μJ, 120 Hz repetition rate, STV-02E-1x0, TEEM photonics, France) was used to excite tissue autofluorescence. A handheld flexible multimode fiber optic probe (3 m long, 365 μm core diameter, FG365UEC; Thorlabs, NJ) was used to guide the excitation light into the tissue and collect tissue autofluorescence to the detection module composed of four spectral bands: 390/40 nm, 470/28 nm, 540/50 nm and 629/53 nm. The

Biomedical Optics EXPRESS

Table 1. Patient demographic characteristics and number of FLIm images and biopsy samples acquired around the tumor resection margins. The number of samples is further divided considering their tissue type according to histopathological evaluation. N-H/L: non-Hispanic/Latino; H/L: Hispanic/Latino.

Subject	Sex	Age	Race	Ethnicity	Number of samples in		
					white matter	gray matter	none
1	M	57	White	N-H/L	4	1	-
2	M	43	Unknown	H/L	5	1	1
3	M	60	Asian	N-H/L	3	3	-
4	F	52	White	H/L	3	-	2
5	F	64	White	N-H/L	4	3	-
6	M	56	White	N-H/L	6	2	1
7	F	69	White	N-H/L	5	-	-
8	M	64	White	N-H/L	5	-	-
9	M	68	White	N-H/L	5	4	-
10	M	55	White	N-H/L	4	1	-
11	M	76	White	N-H/L	4	1	-
12	F	51	White	N-H/L	4	1	-
			Total (new GBM)		**52**	**17**	**4**
13	M	61	White	N-H/L	3	-	1
14	F	60	White	N-H/L	5	1	-
15	M	61	White	N-H/L	5	1	-
			Total (recurrent GBM)		**13**	**2**	**1**
				Total	**65**	**19**	**5**

signal detected at 629/53 nm was of negligible intensity and hence not used for this study. Each spectral band was temporally multiplexed through delay fibers on a single microchannel plate photomultiplier tube (MCP-PMT, R3809U-50; Hamamatsu, Japan) connected to an amplifier (AM-1607-3000; Miteq Inc.) and a high-speed digitizer (12.5 GS/s, PXIe-5185; National Instruments, TX) that sampled the fluorescence decays. The FLIm measurement locations were highlighted with an integrated aiming beam (445 nm continuous-wave solid-state laser, TECBL-50G-440-USB; World Star Tech, Canada) [26]. Tissue exposure to light (UV pulsed laser and blue aiming beam) was kept below the maximum permissible exposure (MPE) allowed by the American Standard for Safe Use of Lasers ANSI Z136.1 [27]. For compliance, the 355 nm laser was used at 1.2 μJ and 120 Hz repetition rate, and the power of the 445 nm laser was 0.25 mW. These values provided a safe dwell time of 5 seconds per location, which was rarely approached.

2.3. Data acquisition

FLIm measurements were acquired *in vivo* from patients undergoing craniotomy procedures for tumor resection. Imaging was achieved by freely scanning the handheld probe across brain tissue (1-3 mm distance between tissue and tip of the probe). Each point measurement comprised a circular surface area with a diameter slightly larger than 365 μm and had a depth that ranged from 150 to 250 μm. The FLIm instrument was connected to a neurosurgical microscope (OPMI Pentero 900; Zeiss, Germany) at the time of surgery, which provided a video stream of the surgical field of view. During tumor resection, FLIm measurements were acquired from 4 to 9 locations along the resection margins selected for biopsy acquisition as part of the surgical procedure. The

Biomedical Optics EXPRESS

neurosurgeon (O.B.) first scanned the area of interest (~ 1 cm^2) with FLIm and subsequently collected the tissue biopsy (2-3 mm^3). This approach enabled a direct co-registration between FLIm data and histopathology results for validation purposes (Fig. 1).

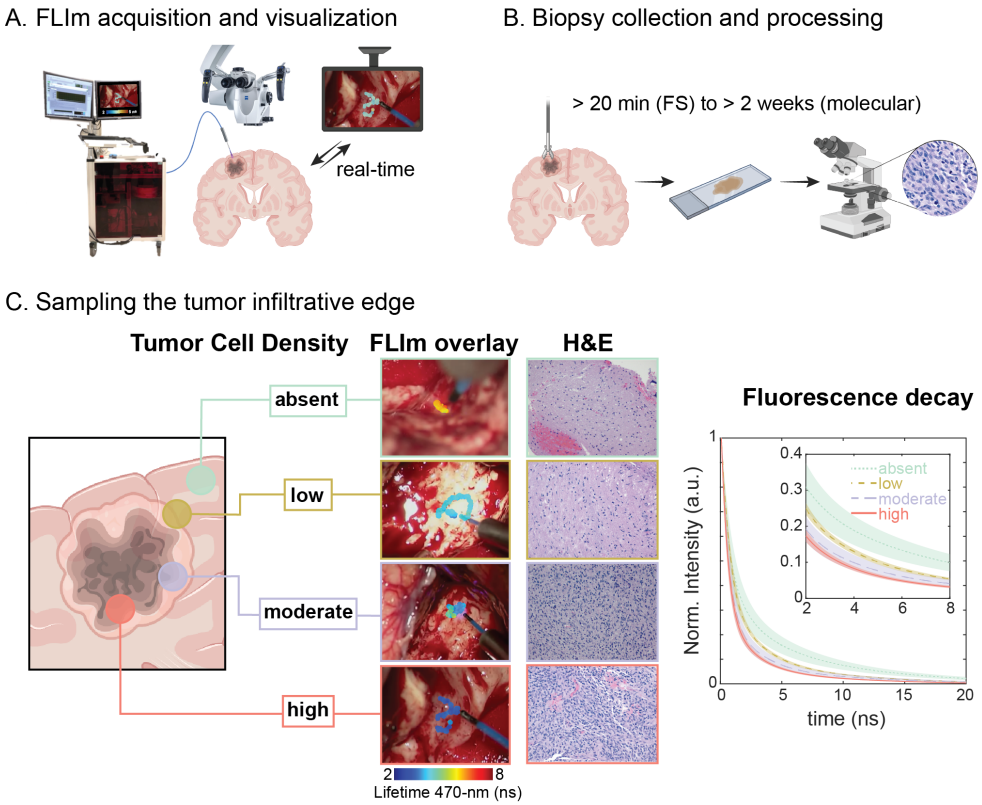

Fig. 1. Experimental setup. a) Schematic of the FLIm acquisition and visualization in the operating room. b) Schematic for biopsy collection and histopathological processing. Results take about 20 minutes at best when frozen sections (FS) are collected - typically one per case. H&E and molecular analysis of all the acquired biopsies are available at least 2 weeks after surgery. c) Schematic of the tumor margin measurements performed around the resection margins showing areas of various degrees of tumor cell density (absent, low, moderate, and high; see Table 2) and corresponding H&E images (obtained with a 20x objective), and a representative fluorescence decay curve for each group.

Table 2. Tumor cellularity density definitions were based on the number of cells per high power field (HPF; 0.5 mm field diameter using a 40x objective) or the percentage of surface covered by tumor nuclei.

Tumor cellularity density	Number of cells per HPF	Surface covered by tumor nuclei
absent	0	0
low	< 200	< 10 %
moderate	200 - 1000	10 - 25 %
high	> 1000	> 25 %

Biomedical Optics EXPRESS

2.4. Data analysis

Every point measurement in a FLIm dataset consisted of three fluorescence intensity decays, one per spectral band. The decays were background subtracted to remove fluorescence generated within the imaging fiber probe and deconvolved with the instrument response function of the system as described elsewhere [28]. Point measurements with a signal to noise ratio below 30 dB were discarded. For every spectral band, the average fluorescence lifetime and signal intensity were extracted from the decay curves with a non-negative least-squared deconvolution with Laguerre expansion method as previously described [29]. The average fluorescence lifetime (τ_{avg}) was defined as the expected value of the probability density function of the decay. The intensity ratio (IR) of each spectral band was computed as a measure of the sample spectral characteristics by dividing each band's intensity by the total sum of intensities.

Each individual sample was used as the unit of analysis, rather than individual point measurements within the sample. Therefore, the analysis reports the mean and standard deviation values of the average fluorescence lifetime and the intensity ratio for each spectral band. Non-parametric tests were used to determine the statistical difference between two (Mann–Whitney U test - null hypothesis: the two samples come from continuous distributions with equal medians) or more groups (Kruskal-Wallis test - null hypothesis: all samples come from the same distribution). p-values below 0.01 were considered statistically significant.

2.5. Tissue characterization through histopathology

Biopsies were evaluated by the neuropathologists (H.S.L.,L.-W.J.) following standard histopathological procedures. Each specimen was assigned a tissue type according to its location in the brain parenchyma (gray or white matter) and a degree of tumor cellularity ranging from absent and low, to moderate and high (Fig. 1(c)). The tumor cellularity density was assessed on a semi-quantitative scale as detailed in Table 2.

The number of samples and point measurements acquired for each tissue type and tumor cellularity group are reported in Table 3. The tissue type of samples with high tumor cellularity was not discernible. Those samples were added to the analysis of both groups (gray and white matter) as reference.

Table 3. Number of samples (number of point measurements) within each tissue type and tumor cellularity density group.

	absent	low	moderate	high
white matter, new GBM	11 (833)	23 (2729)	18 (1312)	4 (223)
gray matter, new GBM	6 (548)	5 (553)	6 (406)	
white matter, recurrent GBM	2 (67)	4 (150)	7 (430)	1 (73)

3. Results and discussion

3.1. FLIm signatures of the GBM infiltrative edge

3.1.1. Influence of the infiltrated tissue type: white matter versus gray matter

Previous studies indicate that endogenous fluorescence from gray and white matter have different lifetime and spectral properties [19,20,23,30]. Such differences were verified on samples with no and low tumor cells and the subsequent analysis was therefore performed separately for samples located in either tissue type (Fig. 2).

White matter free from tumor cells or with low tumor cell density exhibited a longer average lifetime in the mid- and long-spectral bands (470 nm and 542 nm) compared to tumor cellularity-matching samples in gray matter (Fig. 2). At shorter wavelengths (390 nm band) the average

Biomedical Optics EXPRESS

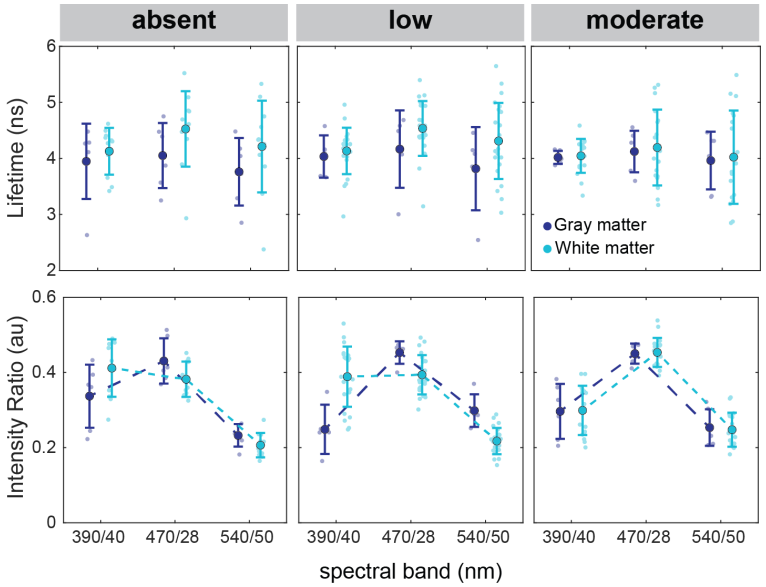

Fig. 2. FLIm parameters variation with infiltrating tissue type. Lifetime and intensity ratio of samples with no, low, and moderate tumor cell presence in gray and white matter, for all spectral bands.

fluorescence lifetime values from both tissue types were comparable. The longer fluorescence lifetime found in white matter may be in part due to contributions from the lipid components of the myelinated axons [23], which are likely excited at 355 nm and their fluorescence extends into the mid and long spectral bands.

In samples with moderate tumor cell density, the fluorescence properties from the tumor cells seemed to dominate the overall fluorescence signal, and on average, the mean fluorescence lifetimes values, as well as the intensity ratios, from both groups became indistinguishable.

The current instrument sampled three spectral bands used as a proxy of the sample's spectral profile. For samples with no or a low number of tumor cells, white matter emission was blue-shifted relative to gray matter. For white matter, the intensity ratio in the 390-nm band was higher or comparable to that in the 470-nm band, whereas for gray matter the highest intensity ratio was found in the 470-nm band. These results align with previous literature that highlight the prominence of NAD(P)H fluorescence in brain tissue [20,31–34]. The red-shifted spectrum of gray matter is likely due to the increased total cell density compared to white matter, which results in more mitochondrial and hence NAD(P)H content [35].

3.1.2. Influence of the tumor cell density

Figure 3 shows the effect of tumor cell density on the fluorescence lifetime and spectral properties for each tissue type. The average fluorescence lifetime of samples in white matter decreased with increasing tumor cell density in the spectral bands centered at 470 nm and 542 nm, although non-significantly. At 390 nm, the average lifetime was comparable across tumor cell densities and only increased, on average, for the samples with the highest cellularity. For samples located in gray matter, the average lifetimes seemed unperturbed by the presence of tumor cells.

For both gray and white matter, however, there was a spectral red shift with increasing tumor cell density. To quantify the red shift, the cumulative density function of the ratio between the intensity at 390 nm and 470 nm was computed (Fig. 3). All scanned tissue with high tumor cellularity had the highest intensity ratio in the 470-nm band ($cdf(I_{390}/I_{470})<1$).For white matter

Biomedical Optics EXPRESS

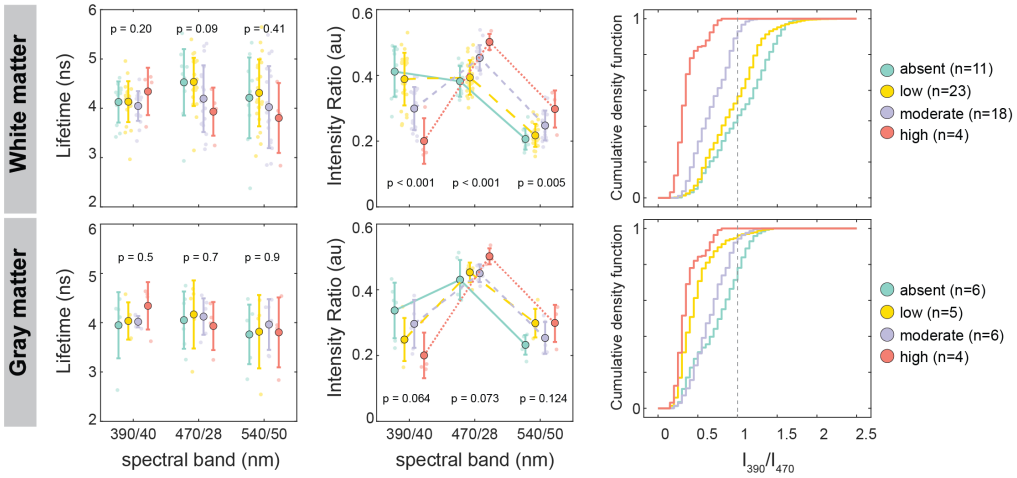

Fig. 3. FLIm parameter variation with tumor cell density. Lifetime, intensity ratio, and cumulative density function (cdf) of the intensity ratio between 390 nm and 470 nm of samples with no, low, moderate, and high tumor cell presence in gray and white matter.

tissue, a point measurement taken in an area with no tumor cells had a 44% probability of having a stronger intensity at the 470-nm band than at the 390-nm band ($cdf(I_{390}/I_{470})<1$). About half of the point measurements acquired from white matter tissue with low tumor cellularity were red-shifted compared to normal white matter ($cdf(I_{390}/I_{470}) = 0.55$) and 91% of point measurements in samples with moderate tumor cellularity had a stronger contribution in the 470-nm band. Point measurements from gray matter were overall red-shifted than those in white matter. 75% of points from pure gray matter tissue had a stronger intensity contribution at 470 nm. Almost all points in the low and moderate tumor cell density groups for gray matter had a dominant signal in this band ($cdf(I_{390}/I_{470}) = 0.96$, and 0.93, respectively).

The current results align with previous studies that performed intensity- or spectral-based fluorescence measurements of human glioblastoma. Most studies report an emission maximum of GBM between 460 and 490 nm that is similar to or red-shifted from that of normal brain [23,30,33,34,36]. However, not all studies found spectral discrimination between the three tissue types (white matter, gray matter, and tumor) [37], and others reported a blue shift in the GBM emission spectrum compared to that of control brain tissue [38,39]. All these studies employed different excitation wavelengths. The excitation wavelength influences the efficiency at which the various intrinsic fluorophores are excited, possibly contributing to the varying results. *In vivo* and *ex vivo* conditions could also influence the fluorescence emission or lifetime values. A red spectral shift was reported *in vivo* compared to *ex vivo* measurements [33]. Another factor leading to disagreements in the reported spectral properties is the distinct spectral sensitivity responses from the different detectors employed in the earlier studies.

Three patients in this study presented with recurrent GBM and history of previous surgery, chemotherapy, and radiotherapy. The FLIm signatures from these patients differed from those of newly diagnosed GBM (see Fig. 3 and Fig. 4). While a rather small number of patients and collected samples were available for the analysis, current results indicate that the lifetimes from samples with previous GBM history were overall longer than those from newly diagnosed GBM patients. Moreover, the lifetime values increased with increasing tumor cellularity (Fig. 4), instead of the decreasing trend observed in newly diagnosed GBMs (Fig. 3). The spectral profile, however, also red shifted with increased cellularity compared to samples with no tumor cells (absent), but no progressive shift was detected between samples from low, moderate and high

Biomedical Optics EXPRESS

tumor cellularity (Fig. 4). The prior surgeries and radio/chemotherapies generated scar tissue and necrosis, as confirmed by pathology. Brain necrosis has been associated with longer lifetime values [19].

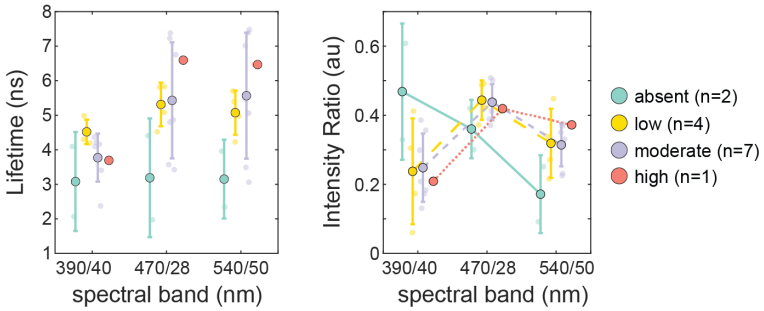

Fig. 4. FLIm parameter variation with tumor cell density of samples from patients with recurrent GBM. Lifetime and intensity ratio of samples with no, low, moderate, and high tumor cell presence infiltrating white matter.

3.2. *Classification ability of intraoperative FLIm: a pilot analysis*

The distinct fluorescence lifetime and spectral properties of GBM and normal tissue indicate that FLIm has the potential to identify tumor tissue around the infiltrative edge. Previous studies have utilized machine learning analysis to discriminate between brain tissue types (white matter and gray matter) and low- and high-grade gliomas [20,30]. In contrast, the goal here was to discriminate between areas of high and low tumor cell density within the surgical resection margins. For this, a linear discriminant analysis (LDA) was performed on a dataset obtained during surgery (*in vivo*) and curated for similar histopathological and clinical characteristics. The classification features considered for this pilot study included the average lifetimes (LT), the intensity ratios (IR), and the Laguerre coefficients (LC) in all three spectral bands. A leave-on-out validation was applied, where all samples from a single patient were omitted from the training set. Due to the low number of gray matter samples available, the analysis was performed only on white matter samples from newly diagnosed GBM patients.

With the current dataset, a multi-class classifier failed to accurately identify the 4 groups of tumor cell density used in this study. The highest degree of confusion was observed between absent and low cellularity samples and between moderate and high cellularity samples, indicating that a binary classifier between normal and tumor samples could yield better results. Three LDA classifier models partitioned the data into "Negative" and "Positive" classes using different tumor cellularity thresholds. Table 4 shows the confusion matrices and performance parameters for each model. The best accuracy (65%) was achieved by the model that considered absent and low tumor cellularity samples as "Negative" and samples with moderate and high tumor cellularity as "Positive" (Table 4(B)), as the results of the multi-class classifier suggested. Partitioning the data between "absent" and all the other groups (Table 4(A)) yielded a high sensitivity (81%), but very low specificity (2%) as a result of many false positives. Thus, the samples free of tumor were incorrectly classified. When only samples with high tumor cell density were considered "Positive" (Table 4(C)), the model performed at high specificity (96%) and low sensitivity (13%). Thus, it had a high rate of false negatives, misclassifying tumor samples as "Negative". With current data, the most accurate detection threshold of intraoperative FLIm was between low and moderate tumor cell density, that is, between 10 and 25% of the surface covered by tumor cells. While this is a first analysis employing a small dataset and a non-optimized classifier, current results suggest that FLIm has the potential to identify the GBM infiltrating edges, in

Biomedical Optics EXPRESS

particular those exhibiting high tumor cellularity. If left behind, such areas could trigger rapid tumor re-occurrence.

Table 4. Confusion matrices and performance of LDA models for varying tumor cellularity thresholds.

A.	Negative (NEG) = absent; Positive (POS) = low + moderate + high					
		Predict				
		POS	NEG	sensitivity	specificity	accuracy
True	POS	81.1%	18.9%	0.81	0.02	0.41
	NEG	98.2%	1.8%			
B.	NEG = absent + low; POS = moderate + high					
		Predict				
		POS	NEG	sensitivity	specificity	accuracy
True	POS	58.2%	41.8%	0.58	0.72	0.65
	NEG	28.2%	71.8%			
C.	NEG = absent + low + moderate; POS = high					
		Predict				
		POS	NEG	sensitivity	specificity	accuracy
True	POS	13.0%	87.0%	0.13	0.96	0.55
	NEG	4.1%	95.9%			

The classification ability of the basic FLIm features was further investigated for the model presented in Table 4(B). A combination of lifetimes, intensity ratios, and Laguerre coefficients achieved the best performance on the LDA model (74% AUC) (Fig. 5). Classification performance dropped when employing lifetimes or intensity ratios alone. The Laguerre coefficients alone performed better than the lifetime and intensity ratios and their combination (AUC = 67%). Independently combining Laguerre coefficients with lifetime or intensity ratios improved the classifier's performance to around 70% AUC.

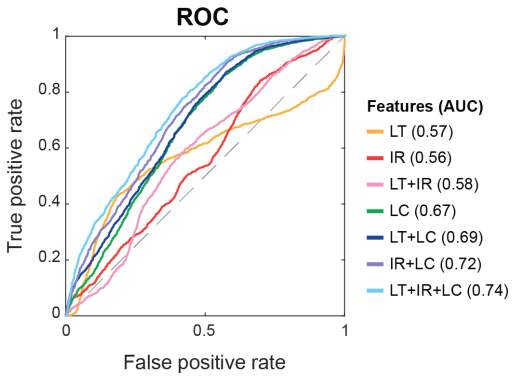

Fig. 5. Classification results of the LDA models with different feature combinations. The classification was performed only on samples from primary GBM on white matter tissue where the positive class contained samples with moderate and high tumor cellularity and the negative class contained samples absent of tumor cells and with low tumor cellularity.

Biomedical Optics EXPRESS

3.3. Limitations and further considerations

The current study needs a bigger and more balanced dataset. The number of data points (observations) in this study was rather low (example, data from white matter tissue: p = 5097 point measurements, from n = 56 samples, from N = 12 patients with newly diagnosed GBM), and unbalanced, with more than double the points in the "Negative" class than the "Positive" class. It is expected that additional data and carefully selected features will improve the performance of the classifiers. Nonetheless, this pilot analysis focused on areas of the infiltrative edge of newly diagnosed GBM patients shows that the intraoperative FLIm device has the potential to identify areas of infiltrating tumor in the brain parenchyma (in white matter in particular). Current results serve as a basis for future studies to demonstrate the ability of intraoperative FLIm for real-time, label-free assessment of surgical margins as an adjunct for tumor resection guidance.

The GBM infiltrative edge is not solely characterized by the tumor cell density. Other parameters may affect tissue autofluorescence and should be considered in upcoming analyses. These include the varying degree of microvascular proliferation and hypoxia around the infiltrative edge [40] and the presence of immune cells in the microenvironment [41].

Further refinement of the validation strategy could yield more specific results. The spatial resolution of the current instrument is limited by the fiber probe (in this study, the probe consisted of a simple multimode fiber without any focusing element). More advanced fiber probe designs compatible with ultraviolet pulse excitation with increased lateral resolution could decrease registration errors. With the current approach, all data with SNR above 30 dB was included in the analysis without considering its spatial distribution. Pre-screening the images to discard points that could lay outside of the biopsy area or off the tissue of interest (i.e., blood pools, or surgical equipment) could further refine the dataset.

4. Conclusion

The fluorescence lifetime signatures of the infiltrative edge of glioblastoma tumors were characterized on a curated set of histopathology-validated samples. To minimize labeling errors, only data from biopsied samples analyzed for tissue type and tumor cell density were included in the analysis. As previously reported [23,30,34], and further verified here (Fig. 2), white and gray matter exhibited significant fluorescence lifetime differences. Thus, to characterize the FLIm signatures of the infiltrative edge, it was important to verify the brain tissue type the tumor infiltrated into. Failing to consider the tissue type resulted in the loss of discrimination power. At the time of surgery, however, the underlying tissue type may not be evident, especially when the tumor nears the eloquent cortex. Surgical neuronavigation may serve as an indication of the most likely tissue type, leading to selecting a FLIm-based classification tuned for white or gray matter.

Samples with different degrees of tumor cellularity exhibited differences in lifetime and intensity ratios that could be missed when grouped together (Fig. 3). As shown in previous reports, low-grade gliomas have shorter lifetimes than normal brain tissue [20], but GBM data appeared with inconsistent trends. Studies measuring glioblastoma fluorescence spectral and lifetime properties acknowledged heterogeneous fluorescence [20], which may be a direct consequence of the tumor's morphological and biochemical heterogeneity [41–43]. Such heterogeneity was also present in the current results (large standard deviation). However, when evaluating the data accounting for similar anatomical and histological characteristics, more consistent trends emerged, highlighting the importance of data curation. Besides separating the datasets into gray and white matter, the previous history of the patient also contributed to increased variability in the FLIm signatures. Samples from patients with recurrent GBM who had undergone surgery and radio-/chemotherapy in the past exhibited distinct FLIm characteristics than newly diagnosed GMBs (Fig. 4), which can partly be explained by contributions of scar tissue and necrotic areas observed in those tumors.

Biomedical Optics EXPRESS

Intraoperative FLIm appears capable of detecting areas of high tumor cell density of the infiltrative edge of GBM tumors (Fig. 5). While the current approach does not provide microscopic resolution to identify single cells, it enables rapid scanning to survey the surgical resection cavity that could lead to in situ and real-time feedback on infiltrations of tumor into brain parenchyma. Eventually, if label-free intraoperative FLIm can predict the tumor cell density in the infiltrative edge in real-time, it would be of great clinical value to optimize the extent of resection for each patient, contributing to better neurosurgical outcomes.

Funding. National Cancer Institute (R01CA250512, P30CA093373).

Acknowledgments. This study was supported by the National Institutes of Health - National Cancer Institute grant R01-CA250512 to L.M. and O.B.the University of California, Davis Comprehensive Cancer Center's Brain Malignancies Innovation Group funded through the Comprehensive Cancer Center Support Grant (P30CA093373). The authors want to thank Dr. Lisanne de Boer, Mr. Roberto P. Frusciante, Dr. Brent Weyers, and Ms. Lisanne Kraft for their assistance with data collection and curation. We also thank Dr. Mirna Lechpammer for setting the basis of the histopathology correspondence analysis. We further acknowledge the assistance and discussions with Dr. Xiangnagn Zhou and Dr. Mohamed Hasan on data analysis. Figures in this report were created with the assistance of Biorender and the *gramm* plotting toolbox [44].

Disclosures. The authors declare no conflicts of interest.

Data availability. Data underlying the results presented in this paper are not publicly available at this time but a deidentified data set may be obtained from the authors upon reasonable request.

References

1. K. D. Miller, Q. T. Ostrom, C. Kruchko, N. Patil, T. Tihan, G. Cioffi, H. E. Fuchs, K. A. Waite, A. Jemal, R. L. Siegel, and J. S. Barnholtz-Sloan, "Brain and other central nervous system tumor statistics, 2021," CA: A Cancer J. for Clin. **71**(5), 381–406 (2021).
2. O. Bloch, S. J. Han, S. Cha, M. Z. Sun, M. K. Aghi, M. W. McDermott, M. S. Berger, and A. T. Parsa, "Impact of extent of resection for recurrent glioblastoma on overall survival," J. Neurosurg. **117**(6), 1032–1038 (2012).
3. M. Lacroix, D. Abi-Said, D. R. Fourney, Z. L. Gokaslan, W. Shi, F. DeMonte, F. F. Lang, I. E. McCutcheon, S. J. Hassenbusch, E. Holland, K. Hess, C. Michael, D. Miller, and R. Sawaya, "A multivariate analysis of 416 patients with glioblastoma multiforme: prognosis, extent of resection, and survival," J. Neurosurg. **95**(2), 190–198 (2001).
4. D. Orringer, D. Lau, S. Khatri, G. J. Zamora-Berridi, K. Zhang, C. Wu, N. Chaudhary, and O. Sagher, "Extent of resection in patients with glioblastoma: limiting factors, perception of resectability, and effect on survival: Clinical article," J. Neurosurg. **117**(5), 851–859 (2012).
5. M. S. Eljamel and S. O. Mahboob, "The effectiveness and cost-effectiveness of intraoperative imaging in high-grade glioma resection; a comparative review of intraoperative ALA, fluorescein, ultrasound and MRI," Photodiagn. Photodyn. Ther. **16**, 35–43 (2016).
6. W. Stummer, A. Novotny, H. Stepp, C. Goetz, K. Bise, and H. J. Reulen, "Fluorescence-guided resection of glioblastoma multiforme utilizing 5-ALA-induced porphyrins: a prospective study in 52 consecutive patients," J. Neurosurg. **93**(6), 1003–1013 (2000).
7. J. Y. K. Lee, J. P. Thawani, J. Pierce, R. Zeh, M. Martinez-Lage, M. Chanin, O. Venegas, S. Nims, K. Learned, J. Keating, and S. Singhal, "Intraoperative Near-Infrared Optical Imaging Can Localize Gadolinium-Enhancing Gliomas During Surgery," Neurosurgery **79**(6), 856–871 (2016).
8. B. Kiesel, M. Mischkulnig, A. Woehrer, M. Martinez-Moreno, M. Millesi, A. Mallouhi, T. Czech, M. Preusser, J. A. Hainfellner, S. Wolfsberger, E. Knosp, and G. Widhalm, "Systematic histopathological analysis of different 5-aminolevulinic acid–induced fluorescence levels in newly diagnosed glioblastomas," J. Neurosurg. **129**(2), 341–353 (2018).
9. M. T. Erkkilä, D. Reichert, J. Gesperger, B. Kiesel, T. Roetzer, P. A. Mercea, W. Drexler, A. Unterhuber, R. A. Leitgeb, A. Woehrer, A. Rueck, M. Andreana, and G. Widhalm, "Macroscopic fluorescence-lifetime imaging of NADH and protoporphyrin IX improves the detection and grading of 5-aminolevulinic acid-stained brain tumors," Sci. Rep. **10**(1), 20492 (2020).
10. C. Senft, A. Bink, K. Franz, H. Vatter, T. Gasser, and V. Seifert, "Intraoperative MRI guidance and extent of resection in glioma surgery: a randomised, controlled trial," The Lancet Oncology **12**(11), 997–1003 (2011).
11. M. A. Pino, A. Imperato, I. Musca, R. Maugeri, G. R. Giammalva, G. Costantino, F. Graziano, F. Meli, N. Francaviglia, D. G. Iacopino, and A. Villa, "New Hope in Brain Glioma Surgery: The Role of Intraoperative Ultrasound. A Review," Brain Sci. **8**(11), 202 (2018).
12. G. W. Auner, S. K. Koya, C. Huang, B. Broadbent, M. Trexler, Z. Auner, A. Elias, K. C. Mehne, and M. A. Brusatori, "Applications of Raman spectroscopy in cancer diagnosis," Cancer and Metastasis Rev. **37**(4), 691–717 (2018).
13. M. Jermyn, K. Mok, J. Mercier, J. Desroches, J. Pichette, K. Saint-Arnaud, L. Bernstein, M.-C. Guiot, K. Petrecca, and F. Leblond, "Intraoperative brain cancer detection with Raman spectroscopy in humans," Sci. Transl. Med. **7**(274), 19–274 (2015).

Biomedical Optics EXPRESS

14. J. Desroches, M. Jermyn, M. Pinto, F. Picot, M.-A. Tremblay, S. Obaid, E. Marple, K. Urmey, D. Trudel, G. Soulez, M.-C. Guiot, B. C. Wilson, K. Petrecca, and F. Leblond, "A new method using Raman spectroscopy for in vivo targeted brain cancer tissue biopsy," Sci. Rep. **8**(1), 1792 (2018).
15. J. Desroches, E. Lemoine, M. Pinto, E. Marple, K. Urmey, R. Diaz, M. Guiot, B. C. Wilson, K. Petrecca, and F. Leblond, "Development and first in–human use of a Raman spectroscopy guidance system integrated with a brain biopsy needle," J. Biophotonics **12**(3), e201800396 (2019).
16. M. Marsden, T. Fukazawa, Y.-C. Deng, B. W. Weyers, J. Bec, D. G. Farwell, and L. Marcu, "FLImBrush: dynamic visualization of intraoperative free-hand fiber-based fluorescence lifetime imaging," Biomed. Opt. Express **11**(9), 5166 (2020).
17. M. Ji, S. Lewis, S. Camelo-Piragua, S. H. Ramkissoon, M. Snuderl, S. Venneti, A. Fisher-Hubbard, M. Garrard, D. Fu, A. C. Wang, J. A. Heth, C. O. Maher, N. Sanai, T. D. Johnson, C. W. Freudiger, O. Sagher, X. S. Xie, and D. A. Orringer, "Detection of human brain tumor infiltration with quantitative stimulated Raman scattering microscopy," Sci. Transl. Med. **7**(309), 163–309 (2015).
18. T. C. Hollon, B. Pandian, and A. R. Adapa, *et al.*, "Near real-time intraoperative brain tumor diagnosis using stimulated Raman histology and deep neural networks," Nat. Med. **26**(1), 52–58 (2020).
19. A. Alfonso-Garcia, J. Bec, S. Sridharan Weaver, B. Hartl, J. Unger, M. Bobinski, M. Lechpammer, F. Girgis, J. Boggan, and L. Marcu, "Real–time augmented reality for delineation of surgical margins during neurosurgery using autofluorescence lifetime contrast," J. Biophotonics **13**(1), e201900108 (2019).
20. P. V. Butte, A. N. Mamelak, M. Nuno, S. I. Bannykh, K. L. Black, and L. Marcu, "Fluorescence lifetime spectroscopy for guided therapy of brain tumors," NeuroImage **54**, S125–S135 (2011).
21. Y. Sun, N. Hatami, M. Yee, J. Phipps, D. S. Elson, F. Gorin, R. J. Schrot, and L. Marcu, "Fluorescence lifetime imaging microscopy for brain tumor image-guided surgery," J. Biomed. Opt. **15**(5), 056022 (2010).
22. S. R. Kantelhardt, D. Kalasauskas, K. König, E. Kim, M. Weinigel, A. Uchugonova, and A. Giese, "In vivo multiphoton tomography and fluorescence lifetime imaging of human brain tumor tissue," J. Neuro-Oncol. **127**(3), 473–482 (2016).
23. M. Lukina, K. Yashin, E. E. Kiseleva, A. Alekseeva, V. Dudenkova, E. V. Zagaynova, E. Bederina, I. Medyanic, W. Becker, D. Mishra, M. Berezin, V. I. Shcheslavskiy, and M. Shirmanova, "Label-free macroscopic fluorescence lifetime imaging of brain tumors," Front. Oncol. **11**, 666059 (2021).
24. P. F. Laura Marcu Daniel Elson, *Fluorescence Lifetime Spectroscopy and Imaging Principles and Applications in Biomedical Diagnostics* (CRC Press, Taylor and Francis Group, 2015).
25. D. R. Yankelevich, D. Ma, J. Liu, Y. Sun, Y. Sun, J. Bec, D. S. Elson, and L. Marcu, "Design and evaluation of a device for fast multispectral time-resolved fluorescence spectroscopy and imaging," Rev. Sci. Instrum. **85**(3), 034303 (2014).
26. D. Gorpas, D. Ma, J. Bec, D. R. Yankelevich, and L. Marcu, "Real-Time Visualization of Tissue Surface Biochemical Features Derived from Fluorescence Lifetime Measurements," IEEE Trans. Med. Imaging **35**(8), 1802–1811 (2016).
27. "ANSI Z136.1 Safe use of Lasers," 978-1-940168-01-2 (1).
28. A. Alfonso-Garcia, J. Bec, B. Weyers, M. Marsden, X. Zhou, C. Li, and L. Marcu, "Mesoscopic fluorescence lifetime imaging: Fundamental principles, clinical applications and future directions," J. Biophotonics **14**(6), e202000472 (2021).
29. J. Liu, Y. Sun, J. Qi, and L. Marcu, "A novel method for fast and robust estimation of fluorescence decay dynamics using constrained least-squares deconvolution with Laguerre expansion," Phys. Med. Biol. **57**(4), 843–865 (2012).
30. W. H. Yong, P. V. Butte, B. K. Pikul, J. A. Jo, Q. Fang, T. Papaioannou, K. L. Black, and L. Marcu, "Distinction of brain tissue, low grade and high grade glioma with time-resolved fluorescence spectroscopy," Front. Biosci. **11**(1), 1255 (2006).
31. S. Avrillier, F. Hor, M. Desgeorges, D. Ettori, and J. R. Sitbon, "XeCl excimer laser-induced autofluorescence spectroscopy for human cerebral tumor diagnosis: preliminary study," Proc. SPIE **1894**, 177–186 (1993).
32. R. Richards-Kortum and E. Sevick-Muraca, "Quantitative optical spectroscopy for tissue diagnosis," Annu. Rev. Phys. Chem. **47**(1), 555–606 (1996).
33. A. C. Croce, S. Fiorani, D. Locatelli, R. Nano, M. Ceroni, F. Tancioni, E. Giombelli, E. Benericetti, and G. Bottiroli, "Diagnostic Potential of Autofluorescence for an Assisted Intraoperative Delineation of Glioblastoma Resection Margins¶," Photochem. Photobiol. **77**(3), 309–318 (2003).
34. P. V. Butte, Q. Fang, J. A. Jo, W. H. Yong, B. K. Pikul, K. L. Black, and L. Marcu, "Intraoperative delineation of primary brain tumors using time-resolved fluorescence spectroscopy," J. Biomed. Opt. **15**(2), 027008 (2010).
35. B. Gerstl, L. F. Eng, R. B. Hayman, and P. Bond, "The lipids of mitochondria of human gray and white matter," Lipids **4**(6), 428–434 (1969).
36. L. Marcu, R. C. Thompson, S. Garde, M. Sedrak, K. L. Black, and W. H. Yong, "Time-resolved fluorescence spectroscopy of human brain tumors," Proc. SPIE **4613**, 183–187 (2002).
37. W. Lin, S. A. Toms, M. Johnson, E. D. Jansen, and A. Mahadevan-Jansen, "In Vivo Brain Tumor Demarcation Using Optical Spectroscopy," Photochem. Photobiol. **73**(4), 396–402 (2001).
38. M. Zanello, F. Poulon, J. Pallud, P. Varlet, H. Hamzeh, G. A. Lahoud, F. Andreiuolo, A. Ibrahim, M. Pages, F. Chretien, F. D. Rocco, E. Dezamis, F. Nataf, B. Turak, B. Devaux, and D. A. Haidar, "Multimodal optical analysis discriminates freshly extracted human sample of gliomas, metastases and meningiomas from their appropriate controls," Sci. Rep. **7**(1), 41724 (2017).

Biomedical Optics EXPRESS

39. F. Poulon, J. Pallud, P. Varlet, M. Zanello, F. Chretien, E. Dezamis, G. Abi-Lahoud, F. Nataf, B. Turak, B. Devaux, and D. Abi Haidar, "Real-time Brain Tumor imaging with endogenous fluorophores: a diagnosis proof-of-concept study on fresh human samples," Sci. Rep. **8**(1), 14888 (2018).
40. B. Oronsky, T. R. Reid, A. Oronsky, N. Sandhu, and S. J. Knox, "A Review of Newly Diagnosed Glioblastoma," Front. Oncol. **10**, 574012 (2021).
41. Q. Wang, B. Hu, and X. Hu, *et al.*, "Tumor Evolution of Glioma-Intrinsic Gene Expression Subtypes Associates with Immunological Changes in the Microenvironment," Cancer Cell **32**(1), 42–56.e6 (2017).
42. M. Hefti, G. v. Campe, M. Moschopulos, A. Siegner, H. Looser, and H. Landolt, "5-aminolevulinic acid induced protoporphyrin IX fluorescence in high-grade glioma surgery: a one-year experience at a single institutuion," Swiss Med. Wkly. **138**, 180–185 (2008).
43. K. H. B. Lam, A. J. Leon, W. Hui, S. C.-E. Lee, I. Batruch, K. Faust, A. Klekner, G. Hutóczki, M. Koritzinsky, M. Richer, U. Djuric, and P. Diamandis, "Topographic mapping of the glioblastoma proteome reveals a triple-axis model of intra-tumoral heterogeneity," Nat. Commun. **13**(1), 116 (2022).
44. P. Morel, "Gramm: grammar of graphics plotting in Matlab," The J. Open Source Softw. **3**(23), 568 (2018).